Material characterisation and constitutive modelling of a tungsten-sintered alloy for a wide range of strain rates

I. Rohr, H. Nahme, K. Thoma, C.E. Anderson

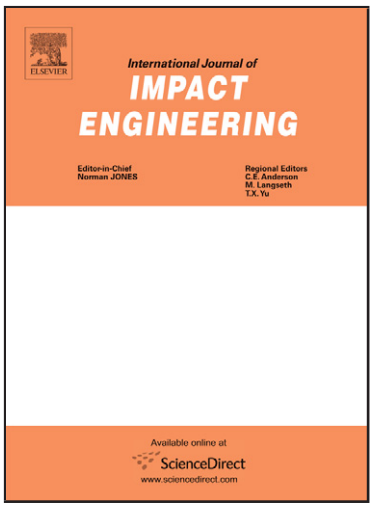

www.elsevier.com/locate/ijimpeng

Material characterisation and constitutive modelling of a tungsten-sintered alloy for a wide range of strain rates

I. Rohr, H. Nahme, K. Thoma, C.E. Anderson Jr.

PII: S0734-743X(08)00029-8
DOI: doi:10.1016/j.ijimpeng.2007.12.006
Reference: IE 1563

To appear in: *International Journal of Impact*

Received date: 18 April 2007
Revised date: 27 December 2007
Accepted date: 27 December 2007

Cite this article as: I. Rohr, H. Nahme, K. Thoma and C.E. Anderson, Material characterisation and constitutive modelling of a tungsten-sintered alloy for a wide range of strain rates, *International Journal of Impact* (2008), doi:10.1016/j.ijimpeng.2007.12.006

Material characterisation and constitutive modelling of a tungsten-sintered alloy for a wide range of strain rates

I. Rohr*, H. Nahme*, K. Thoma* and C. E. Anderson, Jr.+

* rohr@emi.fhg.de, nahme@emi.fhg.de, thoma@emi.fhg.de, *Fraunhofer-Institut für Kurzzeitdynamik, Ernst-Mach-Institut, Eckerstraße 4, 79104 Freiburg, Germany*
+ charles.anderson@swri.org, *Southwest Research Institute, 6220 Culebra Road, San Antonio, Texas 78238-5166, USA*

Abstract

The behaviour of a tungsten-sintered alloy has been investigated using a combination of tension tests, modified Taylor-Impact tests and Planar-Plate-Impact (PPI) tests using VISAR technique. A logarithmic yield stress-strain rate dependency as it is predicted by the original Johnson-Cook (JC) strength model covering a strain rate range of 10 orders of magnitude has been measured. With the PPI tests the Hugoniot-Elastic-Limit and the spall strength, as well as the $U_s - u_p$ relation have been determined. Model parameters for the JC strength model and an equation of state have been determined from the experimental results. The validation of the material model has been performed by numerical simulations of the modified Taylor-Impact tests where an enhanced model validation has been done by comparing the measured and calculated VISAR signals while this technique is normally used for Planar-Plate-Impact tests only.

Keywords: Tungsten; Taylor-Impact test; Planar-Plate-Impact test; VISAR; strain rates; Johnson-Cook

1. Introduction

There is an increased demand for improved material models and their input data when modelling metallic materials under static and dynamic loads. Table 1 provides examples of physical processes and applications and the strain rates associated with the material deformation.

Table 1.

Typical strain rates for different physical processes and applications.

Physical process/application	Velocity [m/s]	Strain rates [s^{-1}]
Quasistatic loading	$<0.1\text{x}10^{-3}$	$<10^{-4}$
Slow forming processes (e.g. rolling, deep drawing)	variable	10^{-3}–10^{2}
Train, car crash	1–70	10^{0}–$5\text{x}10^{2}$
Fast forming processes (e.g. high speed cutting, explosive welding)	variable	10^{3}–10^{6}
Ballistic protection	300–8000	10^{3}–10^{7}
Impact of micrometeorites on satellites/space stations	10000	10^{4}–10^{8}

It should be kept in mind, that in many cases the strain rates given in Table 1 are the values for the beginning of the deformation processes. Even for ballistic events, the strain rates involved may reduce to quasistatic values in the case of non perforation. Therefore, the knowledge of exact model parameters over a wide range of strain rates is absolutely necessary.

There are a great number of constitutive equations available that have been proposed to describe the plastic behaviour of metallic materials as a function of strain rate and temperature. Their objective is to collapse experimental data into one single equation. In this context, a useful model is the Johnson-Cook strength model [12]. In [12] also the way is presented in which the Johnson-Cook model parameters are determined at strain rates ranging from quasistatic to about 400 s^{-1}. In recent years, there was much discussion about the applicability of this equation for the highest strain rates, and thus, various strength models have been developed [e.g. 8, 10, 11, 12, 21, 25, 26, 27, 31]. In this context, some modified versions of the original Johnson-Cook equation have been proposed as well [11, 25]. These strength models differ mainly in the predicted high-strain-rate behaviour especially for strain rates above 10^3 s^{-1} to 10^4 s^{-1}. The significant difference shows that there is definitely a need for a throughout characterisation of all materials which are exposed to such highly dynamic processes.
In this paper, a systematic combination of quasistatic standard tests with enhanced dynamic and high dynamic test methods is presented which have allowed the determination of the strain rate dependency of the yield stress in a strain rate range over 10 orders of magnitude (5 x 10^{-5} to 2.7 x 10^5 s^{-1}) for the investigated tungsten-sintered alloy. The tungsten alloy is representative of materials used for high-density, long-rod projectiles and consists of 92.5 % W, 4.85 % Ni, 1.15 % Fe, and 1.5 % Co. In particular, projectiles made from Hertel-Kennametal material were used in a suite of combined yaw-obliquity experiments reported by Behner et al. [1].

2. Experimental test programmes

2.1 Tensile tests

A standard testing machine was used to conduct tensile tests at different strain rates and one elevated temperature (Fig. 1). The local true stress σ_{true} and true strain ε_{true} values were obtained from the measured stress σ_{tech} and strain ε_{tech} using text book analyses methods.
The force F and the elongation were measured using a load cell and a strain gage, respectively. The true stress at failure was determined from the cross-sectional area A_1 of the specimen after failure and the load (force) at failure. The true strain at failure was determined according to $\varepsilon_{true} = \ln(A_0/A_1)$. By interpolating between the values at the end of the range measured by strain gages which is limited due to the failure of the strain gages at about 5 % strain and the value at failure of the specimen (dotted line), the entire true stress-strain curve has been constructed.

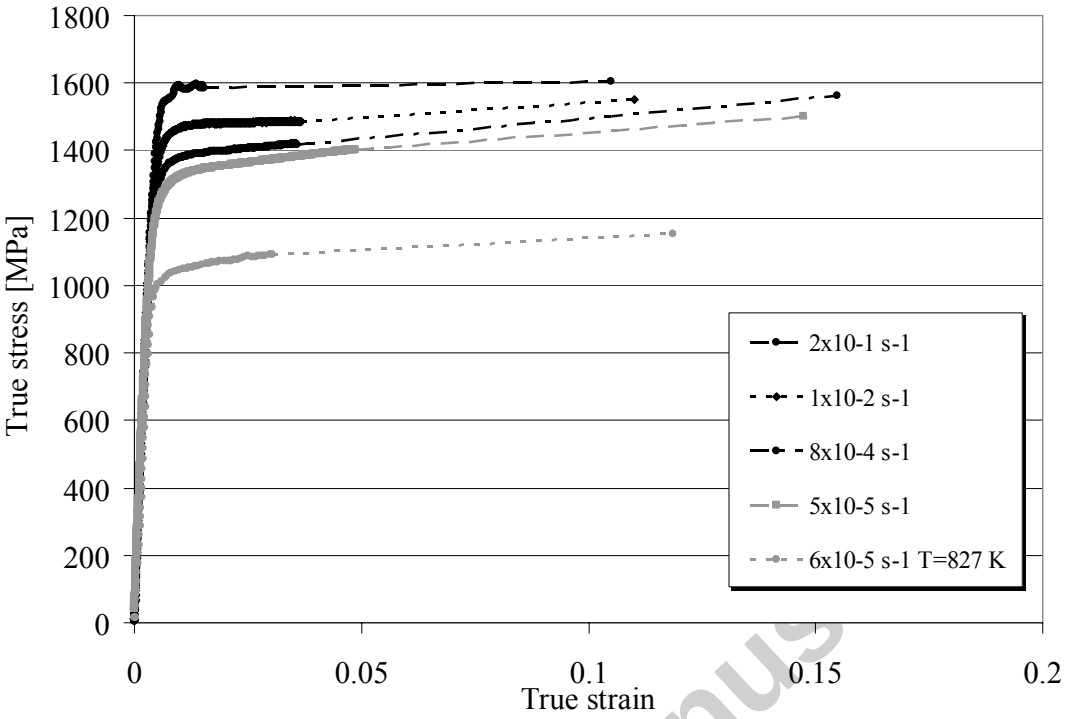

Fig. 1: True stress-strain curves from tensile tests for different strain rates and one elevated temperature.

The material properties deduced from the tensile tests are listed in Table 2.

Table 2.

Material constants at different strain rates for WSA.

Temperature [K]	300	827	300	300	300	300	300	300
Strain rate $\dot{\varepsilon}_{el}$ at yield point σ_Y [s^{-1}]	$5x10^{-5}$	$6x10^{-5}$	$1x10^{-4}$	$8x10^{-4}$	$1x10^{-2}$	$2x10^{-2}$	$2x10^{-1}$	$3x10^{-1}$
Yield stress σ_Y [MPa]	910	880	927	957	1084	1084	1174	1146
Stress σ_f at failure [MPa]	1520	1150	1543	1561	1551	1597	1603	1618
Failure strain	0.15	0.12	0.15	0.16	0.11	0.14	0.11	0.1

The data show that even for the small increase in the strain rate by a factor of two an increase in the stress at failure is evident.

A typical tensile sample from the WSA material and for comparison a typical steel sample [2] exhibiting considerable necking are displayed. In contrast to steel, all WSA samples show no sign of necking at all. Thus, the stress state is uniaxial up to the strain at fracture for the WSA and no corrections with respect to triaxiality (e.g. Bridgman [3]) were necessary.

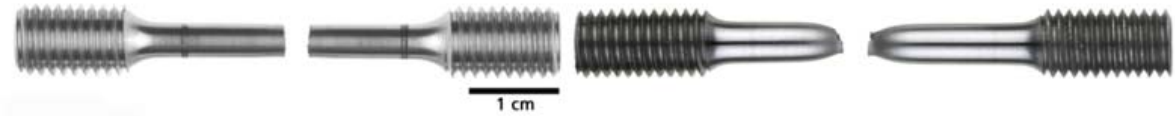

Fig. 2: WSA sample (left) and steel sample (right) for comparison of necking behaviour.

2.2 Modified Taylor-Impact tests

The investigation of the strain rate behaviour in the high strain rate regime $(10^3\,\mathrm{s}^{-1} < \dot{\varepsilon} < 10^4\,\mathrm{s}^{-1})$ was done by a modified Taylor-Impact test using the VISAR technique (invented by Barker and Hollenbach [4]). An extensive description of this technique can be found in Rohr et al. [2, 6].

The experimental setup used is shown schematically in Fig. 3. A steel projectile is accelerated in a single stage gas gun to velocities up to 354 m/s. The projectile then impacts the sample mounted at the end of the gun barrel. The impact velocity is measured using short circuiting pins. The bore diameter of the gun barrel is 70 mm. The cylindrical WSA samples have a length of 50 mm and a diameter of 5 mm (L/D = 10). To avoid plastic deformation, the projectile (i.e. the Taylor anvil) is made of hardened C45 steel (750 HV10). At the rear surface of the sample, the free-surface velocity vs. time profile is measured with a time resolution of 20 ns using a VISAR (Barker [4]).

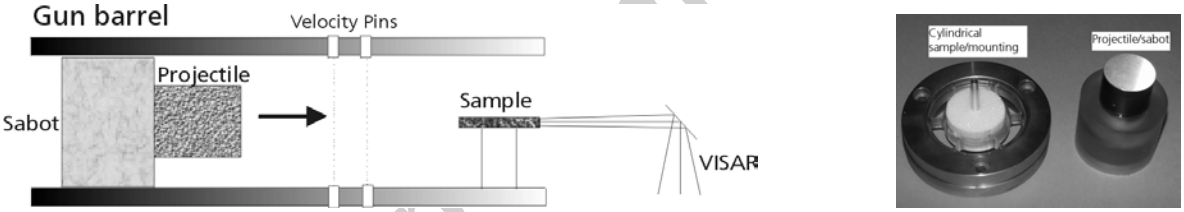

Fig. 3: Experimental setup of the modified Taylor-Impact test with VISAR technique. Projectile/cylindrical sample with its mounting.

Following the one-dimensional theory given by von Karman [7], which describes the material response of rods impacted to loads above the elastic limit, a two-wave structure of the compression wave induced into the sample rod is assumed (von Karman [7], e.g. Zukas [8]). First, an elastic wave propagates along the rod with the longitudinal velocity c_L (= 4405 m/s for WSA), which stresses the material up to the yield point. This elastic wave is followed by a plastic wave with a propagation velocity $v_{pl} << c_L$. This wave plastically deforms the material. So, at a certain time interval after impact, three sample areas can be distinguished:

1. the section stressed to the elastic limit by the elastic wave,
2. the section heavily deformed by the plastic wave, and
3. an intermediate area between both sections which is affected by varying stress, strain and propagation velocity.

The elastic wave accelerates the material and is totally reflected at the free end of the sample rod. The reflected wave propagates back into the sample as a pressure release wave and reduces the pressure stress in the sample to nearly zero. When this release wave reaches the elastic-plastic boundary, a part of the plastic wave will propagate as a new elastic wave into the sample rod because this part of the rod is free of stress at this time. This elastic wave again propagates with the longitudinal sound velocity c_L. As a result of the wave reflection at the rear side of the sample and the generation of new elastic waves at the elastic-plastic boundary, the material of the rod is accelerated stepwise to higher velocities. This is measured as a stepwise increase of the free-surface velocity u_{fs} and is shown schematically in Fig. 4 for an impact from left to right.

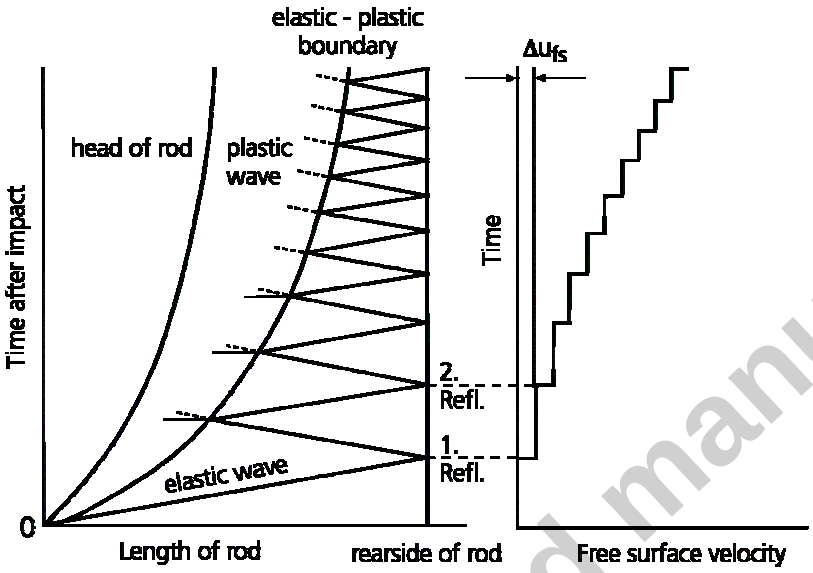

Fig. 4: Wave propagation in a thin rod after impact from left to right.

The determination of the material properties from the measured velocity-time curves is based on the following equations according to Kolsky [9]:

Yield stress: $\sigma_Y = \frac{1}{2} c_L \rho \Delta u_{fs}$ (1)

with the free-surface velocity increase $\Delta u_{fs} = u_{fs1} - u_{fs2}$ at the rear side of the sample.

Strain ($\varepsilon = \partial u / \partial x$) at yield point: $\varepsilon = \frac{u_{fs}}{2c_L} = \frac{u_p}{c_L}$ (2)

Strain rate at yield point: $\frac{d\varepsilon}{dt} = \frac{\Delta\varepsilon}{\Delta t}$ (3)

The original velocity-time curves measured at the rear side of the cylindrical targets for impact velocities between 195 m/s and 354 m/s are shown in Fig. 5. All curves clearly show the stepwise increase described above. Due to dispersion effects, the contour of the steps smears out with subsequent reflections.

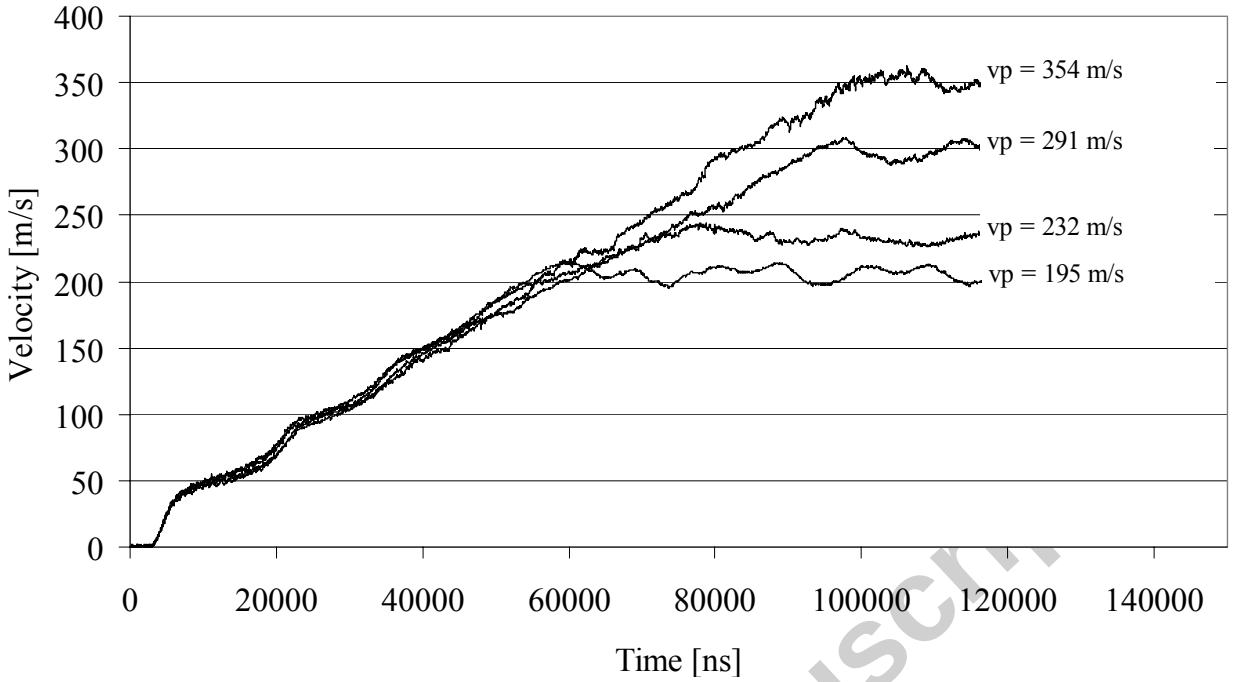

Fig. 5: v-t diagram of 4 inverse Taylor tests at different impact velocities.

The slightly reduced slope of the measured v-t curves for the tests at 291 m/s and 354 m/s can be attributed to the erosion process of the tip of the rods. Due to release waves generated at fracture surfaces and propagating along the sample, erosion typically reduces the particle velocity and thus the measured free-surface velocity. Fig. 6 shows the deformed samples. Sample 2587 is bent due to a second impact.

The yield stress, strain, strain rate and particle velocity, determined according to Eqs. (1) to (3) are listed in Table 3.

Compared to the common Taylor-Impact test analysis given by Taylor [10], the use of the VISAR offers some major advantages. The dynamic material data are determined from the velocity-time history, which is recorded with a typical time resolution of 20 ns. The yield strength determined from a standard Taylor test is influenced by all strain rates ranging from $0 < d\varepsilon / dt < (d\varepsilon / dt)_{max}$. Only data recorded during the deformation process - and not from the distorted post-test sample - allow a definite correlation between yield strength and strain rate. Additional advantages of this test method arise when it is combined with numerical simulations (Rohr et al. [6], see Chapter 3).

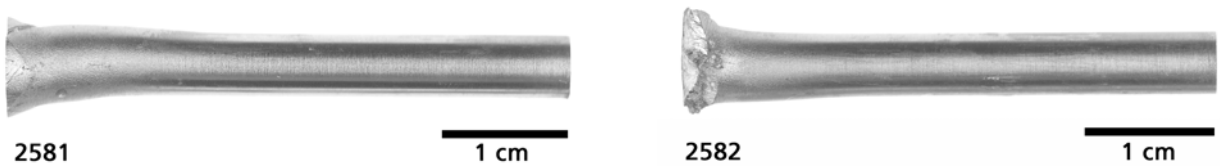

Fig. 6: Deformed samples for 195 m/s, 232 m/s, 291 m/s and 354 m/s.

Table 3.

Dynamic material data determined from Taylor-Impact tests.

v_p [m/s]	u_{fs} [m/s]	u_p [m/s]	σ_Y [MPa]	ε [10^{-3}] at yield point	$d\varepsilon/dt$ [s^{-1}] at yield point
195	37.2	18.6	1458	4.2	1446
232	38.0	19	1489	4.3	1457
291	38.5	19.25	1509	4.4	1476
354	38.5	19.25	1509	4.4	1476

Enhanced validation calculations of the conducted tests can be done since the diagnostics provide a velocity-time signal in addition to the final shape of the specimen. These can be used for a better development and validation of material models for numerical simulations.

2.3 Planar-Plate-Impact tests (PPI)

The technique used to determine the material properties at strain rates $d\varepsilon/dt > 10^5\ s^{-1}$ was the Planar-Plate-Impact test in combination with the VISAR technique, which is described in more detail in Barker et al. [4], Nahme et al. [5], Arnold [11]. The experimental setup is shown in Fig. 7.
Plane parallel samples of 2 mm thickness were impacted by 1 mm thick plane parallel projectile plates at velocities between 416 m/s and 1174 m/s. As in the case of the modified Taylor-Impact tests, the projectile plates were accelerated by means of a single stage gas gun, operated as compressed air gun for impact velocities below 500 m/s and as a powder gun for velocities above 500 m/s. Fig. 8 shows the velocity profiles from the plate impact tests at different impact velocities. Time resolution of the tests was 2 ns/point.

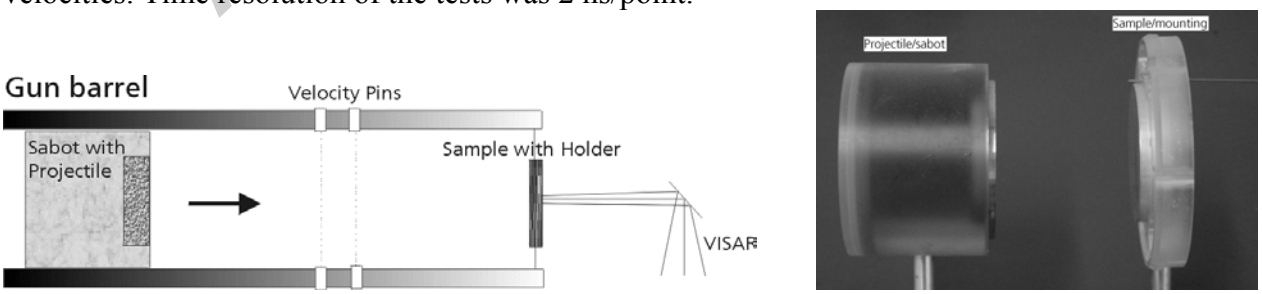

Fig. 7: Left: Experimental setup of Planar-Plate-Impact test (schematic). Right: Projectile with sabot and sample with holder.

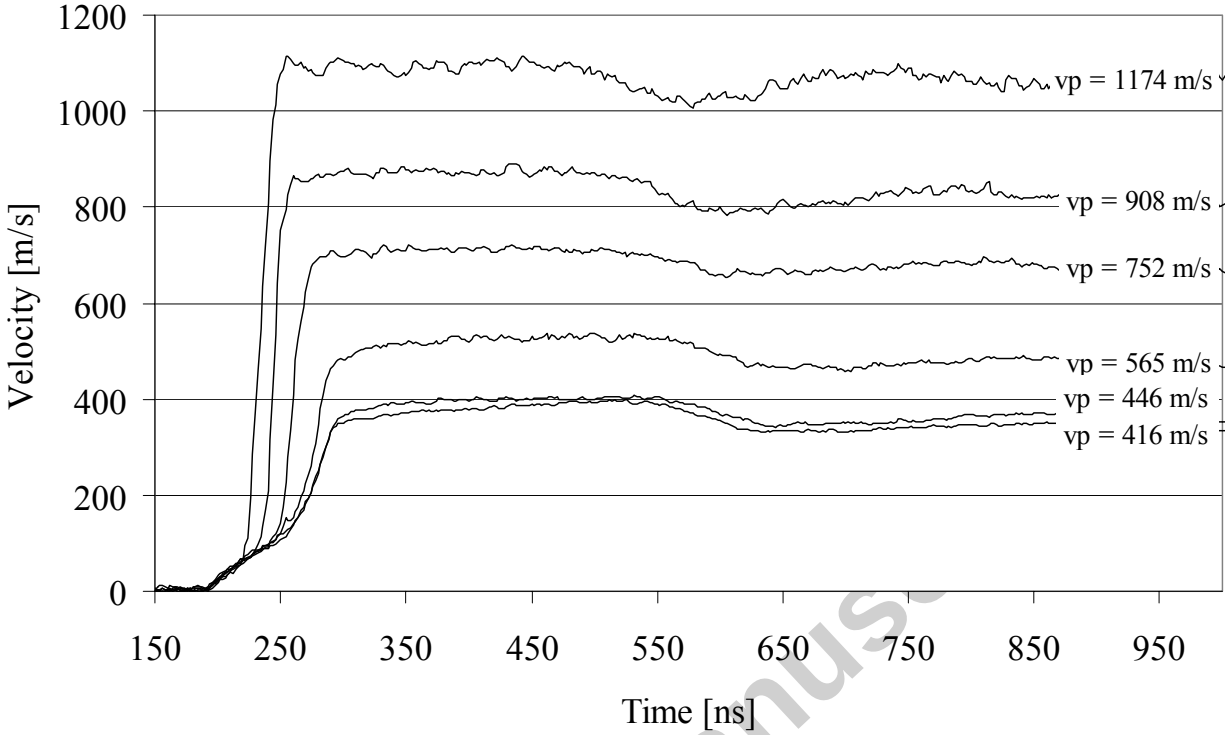

Fig. 8: v-t diagram of 6 plate impact tests at impact velocities between 416 m/s and 1174 m/s.

The dynamic material data were determined from the velocity curves using standard data reduction methods described in detail by Rohr et al. [2]. From the measured velocity-time profiles within the accuracy of the measurements the same strain rate of 2.7×10^5 s^{-1} for the elastic deformation and a Hugoniot-Elastic-Limit (σ_{HEL}) of 2.51 ± 0.13 GPa have been determined for all tests. This dynamic yield stress for three dimensional stress state conditions has been transformed to one dimensional σ_Y-data using the relation

$$\sigma_Y = \frac{1-2\nu}{1-\nu}\sigma_{HEL} \tag{4}$$

given by Jones [13] with a Poisson ratio ν of 0.28 for this tungsten-sintered alloy. The Poisson ratio has been calculated from Young's modulus determined from the quasistatic tension tests and the measured wave velocities using the relations between the moduli and the wave velocities as presented in Kohlrausch [34].

The spall strength shows a quite large variation of 2.3 GPa<σ_{sp}<4.6 GPa and no clear dependency on the impact velocity is visible. So, an average spall strength of 3.5 GPa was used for the numerical simulations described in the following section.

3 Validation Calculations

3.1 Johnson-Cook strength model

Most computational models express the equivalent (von Mises) tensile flow stress as a function of the equivalent plastic strain, strain rate, temperature, and/or pressure. The Johnson-Cook model [15] expresses the equivalent tensile flow stress as

$$\sigma = \left(A + B\varepsilon^{n}\right)\left(1 + C\ln\dot{\varepsilon}^{*}\right)\left(1 - T_{*}^{m}\right) \tag{5}$$

where ε is the equivalent plastic strain, $\dot{\varepsilon}^{*} = \dot{\varepsilon}/\dot{\varepsilon}_{0}$ is the dimensionless plastic strain rate with $\dot{\varepsilon}_{0} = 1\,\mathrm{s}^{-1}$, and $T_{*} = \left(T - T_{300}\right)/\left(T_{melt} - T_{300}\right)$ is the homologous temperature. The constant A represents the yield stress for $\dot{\varepsilon}^{*} = 1$ and $T = T_{300}$. B and n represent the effect of strain hardening. C is the strain rate constant and m characterises the thermal softening.
The determination of the Johnson-Cook model parameters is described for a range of strain rates from quasistatic to about 400 s^{-1} in [15]. In recent years there has been much controversial discussion (e.g. [8, 20]) whether this equation represents the correct material behaviour for the highest strain rates. Indeed, Johnson et al. [16] included a high-strain-rate modification to capture the high-rate response for a high-strength steel. Many different constitutive equations, some of which are microstructurally based, have been developed and can be found in literature e.g. Refs. [17 to 24]. A comparison between the Johnson-Cook model and the Zerilli-Armstrong model is presented in Dey et al. [33]. In addition, for strain rates above a few $10^{3}\,\mathrm{s}^{-1}$, data from Hopkinson-bar experiments - the most widely used test method for the determination of dynamic material data - become questionable [21, 25], and other methods suitable for high strain rates should be used [2, 6].

Nevertheless, the Johnson-Cook model is widely used; thus, Johnson-Cook constitutive parameters are determined from the experimental data. The material characterisation procedure, as described in [2] for a German armour steel, is applied to the WSA and permits a determination of the Johnson-Cook strength model parameters. The procedure and the results for WSA material are presented in the following subsections.

3.2 Determination of Johnson-Cook model parameters

Combining the results of tensile tests, modified Taylor-Impact tests and Planar-Plate-Impact tests, we have determined the yield stress-strain rate dependence covering a strain rate range of 10 orders of magnitude (Fig. 9). In addition to the data for the WSA, also the yield stress-strain rate dependency of German armour steel taken from Ref. [2] is shown. In contrast to the steel, the WSA investigated here can be described very well using a linear behaviour on a logarithmic strain rate scale as it is shown in Fig. 9. Thus, as far as the yield stress dependency is concerned, the Johnson-Cook model is applicable to describe this material behaviour, and no modification of the model as described e.g. in [32] has to be used for WSA. From the logarithmic fit to the data the Johnson-Cook parameters A and C have been deduced as given in Table 4.

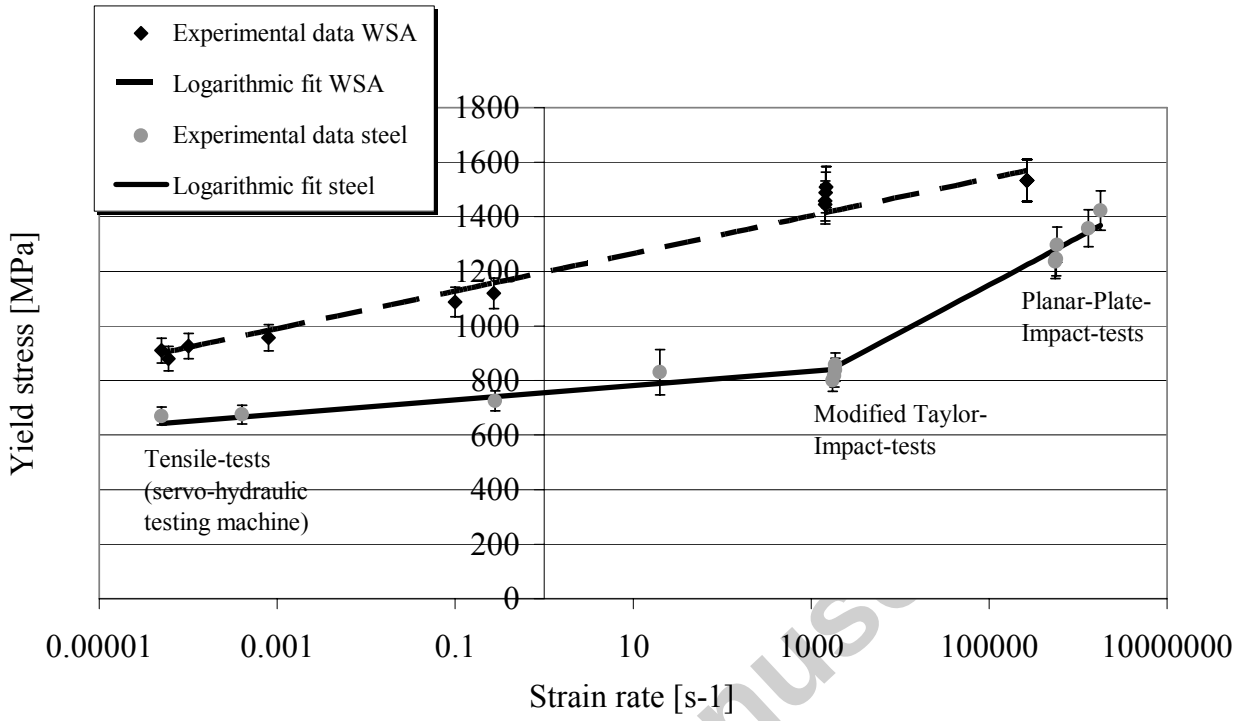

Fig. 9: Yield stress-strain rate diagram and logarithmic curve fit of WSA, data of HZB/L-armour steel are shown for comparison.

In Fig. 10 the true stress-strain curves for (exemplarily) three different strain rates ($2 \times 10^{-1}\ s^{-1}$, $1 \times 10^{-2}\ s^{-1}$, $8 \times 10^{-4}\ s^{-1}$) and the high temperature data are shown. It can be seen that the stress-strain curves clearly depend on the strain rate. At lower strain rates, the true stress-strain curve exhibits a definite strain hardening, whereas at higher strain rates, the stress-strain curve shows a more elastic-ideal-plastic behaviour with very little strain hardening, which is typical of high hardened materials. In contrast to the yield stress-strain rate dependency, this behaviour cannot exactly be described by the Johnson-Cook model. Nevertheless, to determine the best fit, the stress-strain curves were fitted to represent the elastic-ideal-plastic material behaviour at higher strain rates as shown in Fig. 10. This seems appropriate because 1) this elastic-ideal-plastic behaviour is expected at higher strain rates, 2) generally, the amount of strain hardening of the tungsten alloy is very small compared to the strain independent yield stress.

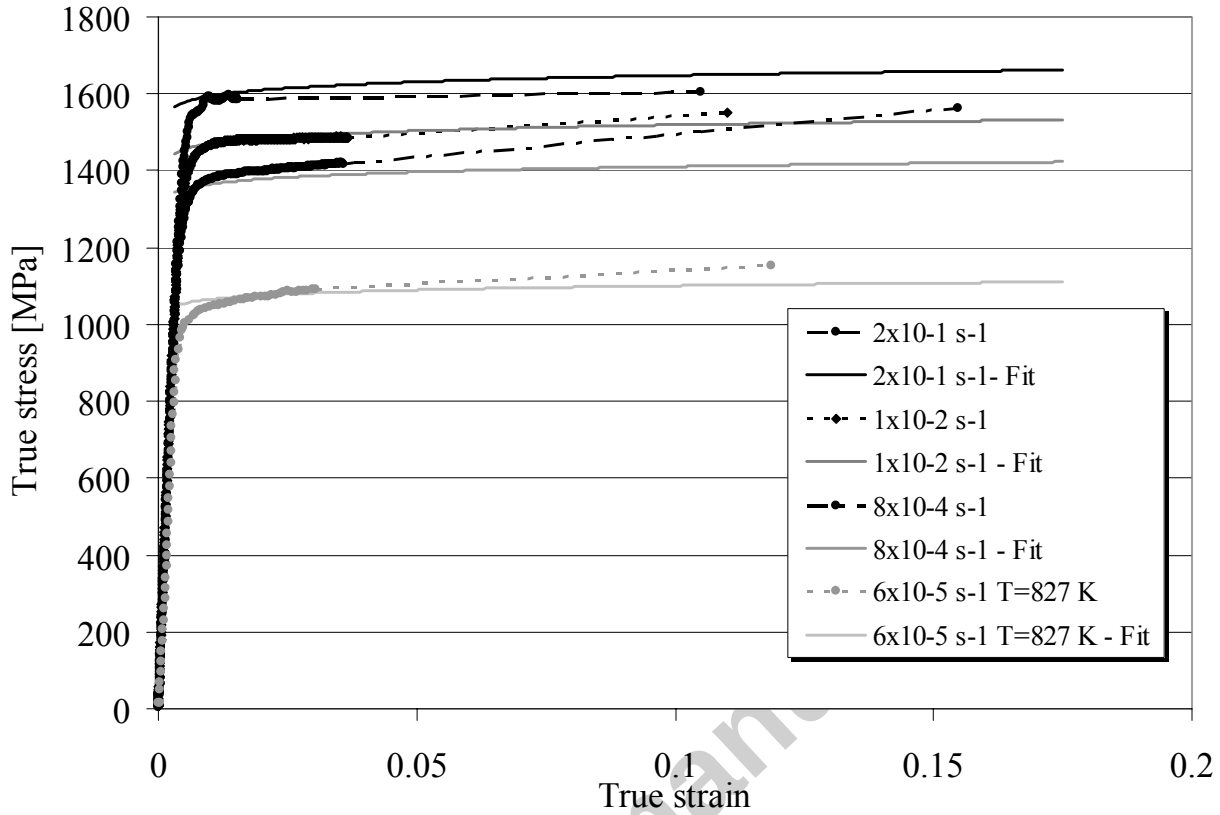

Fig. 10: True stress-strain curves and fit of WSA at low strain rates.

The Johnson-Cook parameters for the tungsten-sintered alloy are given in Table 4.

Table 4.

Johnson-Cook constitutive parameters.

A	**B**	**n**	**C**	**m**
1197 MPa	580 MPa	0.05	0.025	1.9

3.3 Equation of state (EOS)

To characterise the plastic material behaviour at high pressures typical for highly dynamic processes, a relation between the hydrostatic pressure p, the local density ρ (or specific volume) and local specific energy e (or temperature) is needed. This relation is known as equation of state (EOS). Theoretically, an EOS can be determined from the thermodynamic properties of the material and ideally should not require dynamic data. In practice, however, the way to establish an EOS is to perform well-characterised dynamic experiments. It is important to recognise that, since the relationship is required for the use in a numerical code, an analytic form gives computational efficiency. Such an analytic form is at best an approximation to the true relationship.

The most commonly used reference curve to establish a Mie-Grueneisen equation of state for solid materials is the shock Hugoniot. The Rankine-Hugoniot equations for shock conditions can be regarded as defining a relation between any pair of the variables ρ, p, e, the particle velocity u_p and the shock velocity U_s. In many dynamic experiments measuring u_p and U_S, it has been found that for most solids and many liquids an empirical linear relationship $U_S = c_B + Su_p$ exists between those two variables over a wide range of pressure, with the bulk sound speed c_B and the slope of the relation S being material constants. From the Planar-Plate-Impact experiments presented in chapter 2.3 this relation has been determined as $U_S = 1.3684u_p + 4066.2\text{m/s}$ (Fig. 11).

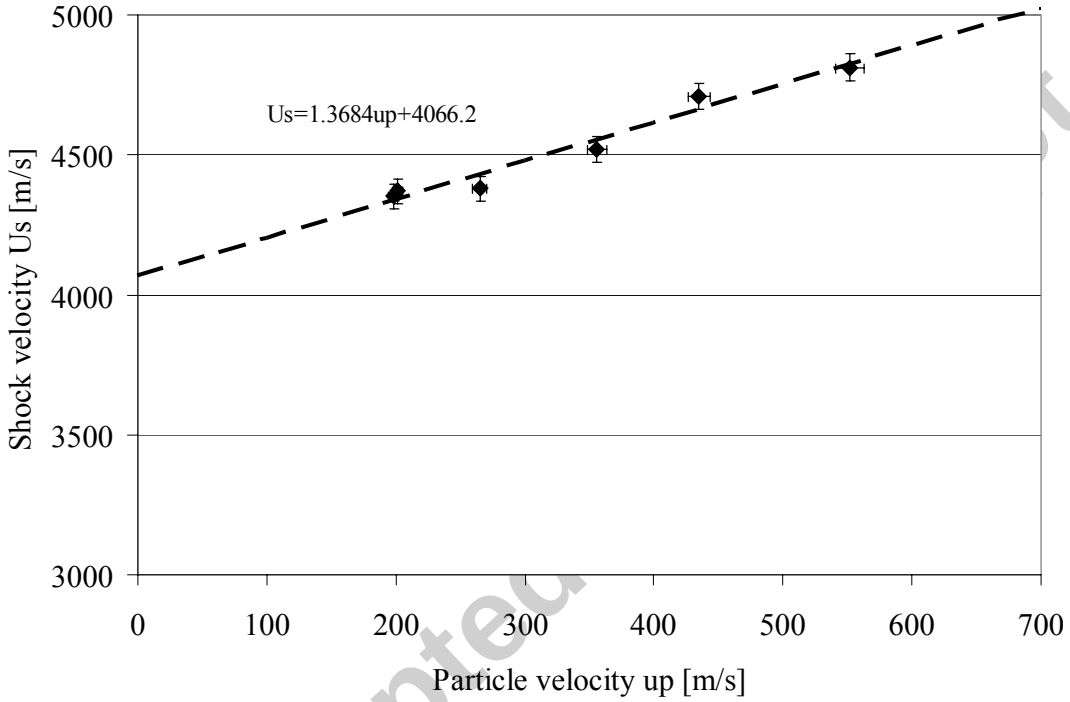

Fig. 11: Shock velocity vs. particle velocity diagram with linear fit for WSA.

3.4 Other material properties

The aim of the work presented here is not the modelling of fracture behaviour of WSA. Several more or less complex models can be found in literature (e.g. Johnson et al. [31]) where more or less complex tests (e.g. tensile tests with different notched specimen) have to be done. Due to the fact that the focus in this paper lies on the experimental results and strength modelling for a wide strain rate range, only a simple approach for modelling material failure is used where failure is initiated if any one of the maximum tensile principal stress or tensile strain in principal stress direction exceeds its specific limit. With this simple approach, the failure which occurs in the Taylor-Impact tests and spall failure in Planar-Plate-Impact tests can be reproduced.

The failure model parameters for numerical simulations were deduced from the failure strains at low strain rates at 300 K and 827 K (Fig. 12) and from the spall strength determined with the Planar-Plate-Impact tests. Despite a large variation in the data, there is a decreasing failure strain with increasing strain rate. Extrapolating the logarithmic fit of Fig. 12 results in a very low failure strain (around 5 %) at strain rates between 10^3 s^{-1} and 10^4 s^{-1}. Nevertheless, the numerical simulations of the modified Taylor-Impact tests have shown, that a mean value of 5 % failure

strain is much too low. To yield good agreement between experimental and numerical results, a failure strain of 120 % was necessary. The presumption is a stress state dependent behaviour of the WSA as it has been shown for several materials previously (e.g. [31]). This behaviour is characterised by high failure strains (above 100 %) in the hydrostatic regime and low failure strains for positive states of stress triaxiality. As mentioned above, a simple tensile-failure criterion with a value of 3500 MPa for tensile failure was used to model the spallation. 3500 MPa was simply taken as the mean value of the measured spall stresses in chapter 2.3.

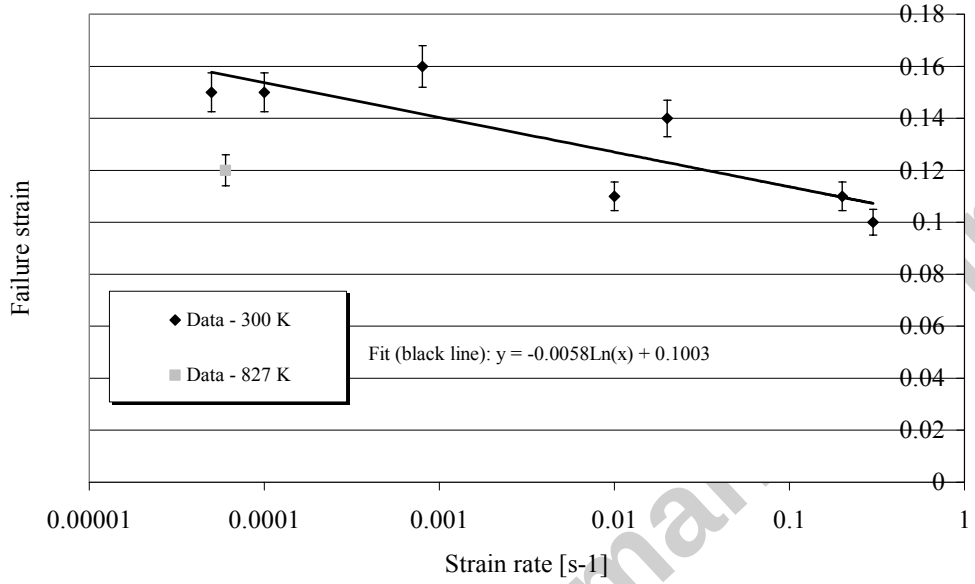

Fig. 12: Failure strain for different strain rates at room temperature (black dots) and for 827 K (grey dot).

Other important material properties provided by the manufacturer of the WSA or having been determined for the WSA are given in Table 5. The friction coefficient was estimated according to Kuchling [30].

Table 5.

Material properties.

Shear modulus G [GPa]	Young's modulus E [GPa]	Longitudinal sound velocity in semi-infinite target c_p [m/s]	Longitudinal sound velocity in long rods c_L [m/s]	Density [g/cm^3]	Friction coefficient	Poisson ratio
134	343	5160	4405	17.68	0.2	0.28

3.5 Simulation of modified Taylor-Impact tests

All simulations were carried out using the two-dimensional hydrocode AUTODYN-2D [27], and Lagrangian coordinates were used to describe both the projectile and the target. Due to the fact that 1) with the exception of the parameter C all other parameters of the JC model have been

deduced from tensile tests and 2) the determination of the parameter C is independent of the modified Taylor-Impact test data (because of the logarithmic slope of the fit presented in Fig. 9), validation calculations to check the elastic-plastic behaviour of the material which is represented by the Johnson-Cook strength model and the equation of state can be done by comparing the VISAR signal only.

The input data for the numerical simulations are given in Table 6. To represent the high hardness of the steel projectile, an elastic strength model was chosen. The shock equation of state for the C45-steel was taken from [29]. The linear relationship

$$U_s = 4483\text{m/s} + 1.332u_p \tag{6}$$

was determined from Planar-Plate-Impact tests.

Table 6.

Material model used in the numerical simulations.

Model/Parameter	**Target: tungsten-sintered alloy**	**Projectile: C45 steel**
EOS:		
Density [g/cm^3]	17.68	7.8
Parameter c_B [m/s]	4066.2	4483
Parameter S	1.368	1.332
Grueneisen coefficient	1.736	1.664
Reference Temp. [K]	300	300
Spec. heat [J/kgK]	134	420
Strength model:	Johnson-Cook	Elastic
A [MPa]	1197	
B [MPa]	580	
n	0.05	
C	0.025	
m	1.9	
Shear modulus [kPa]	134x10^6	81x10^6
Melt. Temp. T_m [K]	1730	
Failure parameters		
Principal stress [MPa], strain	3500, 1.2	

Depending upon the impact velocity, considerable plastic deformation and failure can occur in such experiments, which exhibit multiaxial stress states with strain rates exceeding 10^5 s^{-1} and strains in excess of 2. An evaluation of the model and data can be made by comparing the computed results with data from cylinder impact tests [15]. The parameters presented in Table 5 and Table 6 are used as input data for the numerical simulations.

As mentioned before, the final length of the specimen was used to calibrate the failure strain with a constant value of 120 %. Nevertheless, the elastic-plastic behaviour which is shown in the velocity-time plot can be used for the validation of the Johnson-Cook strength model and the equation of state.

A view of the cross section of the geometric simulation model along the axis of symmetry is presented in Fig. 13. The free-surface velocity-time profile is recorded at the reference point at the target (rod) rear surface.

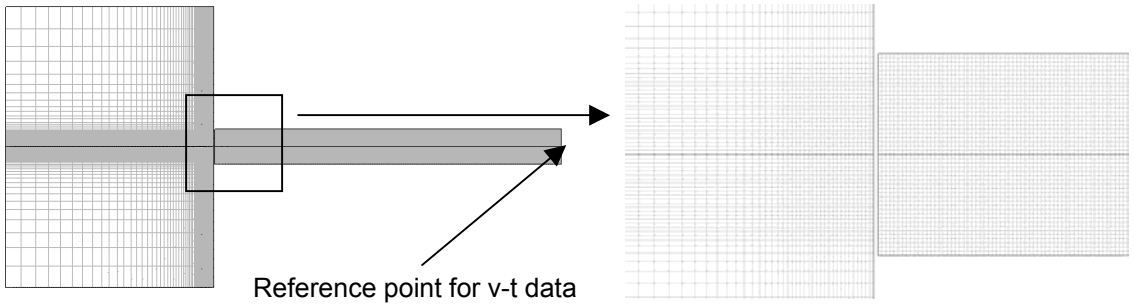

Fig. 13: View of the cross section of the geometric simulation model along the axis of symmetry.

Fig. 14 shows the measured free-surface velocity-time histories together with the curves from the numerical simulations. For all impact velocities the characteristic slope of the curves shows a quantitatively good agreement between the experimental and calculated data. This agreement is remarkable because this comparison is a much more sensitive way of model validation than the usual comparison of the measured and calculated deformation only.

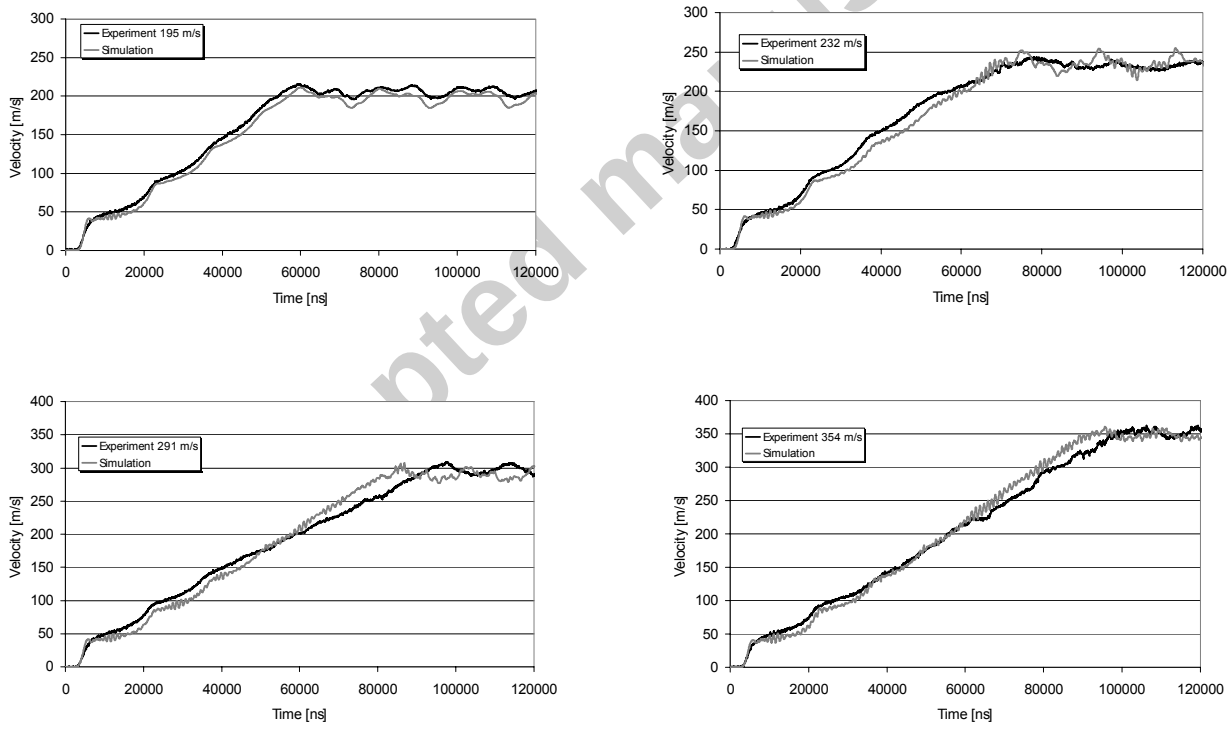

Fig. 14: Comparison of simulated and measured free-surface velocity-time curves from the modified Taylor-Impact tests at different impact velocities for WSA.

4 Summary and Conclusions

A tungsten-sintered alloy has been characterised over a wide range of strain rates following a methodology developed in Refs. [2, 6, 26] for steel. The systematic combination of standard measurement techniques (tensile tests) with dynamic material tests (modified Taylor-Impact tests with VISAR technique and Planar-Plate-Impact tests with VISAR) made it possible to determine the strain rate dependency of the yield stress in a strain rate range over 10 orders of magnitude (5×10^{-5}-2.7×10^{5} s^{-1}). The fit curve to these experimental yield stress-strain rate data shows a consistent logarithmic slope over the whole strain rate range where no steeper increase at higher strain rates could be observed for the WSA. Therefore, two conclusions can be drawn: 1) In contrast to other metals as presented e.g. in Krüger et al. [35] for Ti or Rohr et. al. for steel [2], no change in the microstructural rate controlling mechanism at high strain rates appears for the WSA. 2) The JC strength model is an appropriate choice for the numerical modelling of the material. This has been validated by numerical simulations of the modified Taylor-Impact tests.

5. References:

[1] Behner, Th., Hohler, V., Anderson, Jr. C.E., and Goodlin, D.L. Influence of yaw angle on the penetration reduction of long rods in oblique targets. In: Proc. 20th Int. Symp. on Ballistics 2, Lancaster, PA, Destech Publications, 2002, pp. 834-841.

[2] Rohr, I., Nahme, H., Thoma, K. Material characterization and constitutive modelling of ductile high strength steel for a wide range of strain rates. Int. J. Impact Engng., 2005, 31, pp. 401-433.

[3] Bridgman, P. Studies in large plastic flow and fracture. Harvard University Press, Cambridge, MA 1964.

[4] Barker, L.M., Hollenbach, R.E. Laser interferometer for measuring high velocities of any reflecting Surface. J. Appl. Phys., 1972, 43, pp. 4669-4675.

[5] Nahme, H., Worswick, M.J. Dynamic properties and spall plane formation of brass. In: Proc. Eurodymat 1994, Oxford, UK, pp. 707-712.

[6] Rohr, I., Nahme, H., Thoma, K. A modified Taylor-Test in combination with numerical simulations - a new approach for the determination of model parameters under dynamic loads. J. Phys. IV France, 2003, 110, pp. 513-518.

[7] Von Karman, T., Duwez, P. The propagation of plastic deformation in solids. J. Appl. Phys., 1950, 21, pp. 987-994.

[8] Zukas, J., Nicholas, T., Swift, H., Greszcuk, L., Curran, D. Impact dynamics. Krieger Publ. Comp., Malabar, Florida, 1992.

[9] Kolsky, H. Stress waves in solids. New York, Dover Publications, 1963.

[10] Taylor, G.I. The use of flat-ended projectiles for determining yield stress. Proc. Roy. Soc., London, 1948, pp. 289-299.

[11] Arnold, W. Dynamisches Werkstoffverhalten von Armco-Eisen bei Stoßwellenbelastung. PhD-thesis. Technical University Munich, 1991.

[12] Romanchenko, V.I., Stepanov, G.V. Dependence of the critical stresses on the loading time parameters during spall in copper, aluminum and steel. J. Appl. Mech. and Tech. Phys., 1980, 21, pp. 555-561.

[13] Jones, O.E. Shock wave mechanics. In: Rohde, R.W., Butcher, B.M., Holland, J.R., Karnes, C.H., editors. Metallurgical effects at high strain rates. Plenum Press, 1973, pp. 33-55.

[14] Chen, W.F., Han, D.J. Plasticity for structural engineers. ISBN 0387-96711-7. Springer-Verlag, 1988.

[15] Johnson, G.R., Cook, W.H., 1983. A constitutive model and data for metals subjected to large strains, high strain rates and high temperatures. Proc. 7th Int. Symp. on Ballistics: Den Haag, 1988, pp. 541-547.

[16] Johnson, G.R, Holmquist, T.J. Anderson, C.E. Jr., and Nicholls, A.E. Strain-rate effects for high-strain computations. J. de Physique IV, 2006,134, pp. 391-396.

[17] Borvik, T., Langseth, M., Hopperstadt, O.S., Malo, K.A. Ballistic penetration of steel plates. Int. J. Impact Engng., 1999, 22 (9-10), pp. 855-886.

[18] El-Magd, E. Mechanical properties at high strain rates. J. Phys. IV, 1994, C8 (III-4), pp. 149-170.

[19] Holmquist, T.J., Johnson G.R. Determination of constants and comparison of results for various constitutive models. J. Phys. IV, 1991, C3 (III-1), pp. 853-860.

[20] Meyers, M.A. Dynamic behavior of materials. New York: Wiley, 1994.

[21] Rule, W.K., Jones, S.E. A revised form for the Johnson-Cook strength model. Int. J. Impact Engng., 1998, 21 (8), pp. 609-624.

[22] Steinberg, D.J., Cochran, S.G., Guinan, M.W. A constitutive model for metals applicable at high-strain rate. J. Appl. Phys., 1980, 51 (I), pp. 1498-1504.

[23] Steinberg, D.J., Lund, C.M. A constitutive model for strain rates from 10^{-4} to 10^{6} s^{-1}. J. Appl. Phys., 1989, 65 (II), pp. 1528-1533.

[24] Zerilli, F.J., Armstrong, R.W. Dislocation-mechanics-based constitutive relations for material dynamics calculations. J. Appl. Phys., 1987; 61, pp. 1816-1825.

[25] Lindholm, U.S. Dynamic deformation of metals. Proceedings of the Colloquium on Behavior of Materials under Dynamic Loading at the Winter Annual Meeting of ASME, Chicago, USA, 1965.

[26] Rohr, I. Integrale Charakterisierung und Modellierung von duktilem Stahl unter dynamischen Lasten. PhD-thesis. Universität der Bundeswehr München, 2003.

[27] Century Dynamics. Autodyn Theory Manual. Century Dynamics Ltd., Horsham, 2002.

[28] Hiermaier, S., Riedel, W., Hayhurst, C.J., Clegg, R.A., Wentzel, C.M. Advanced material models for hypervelocity impact simulations. Fraunhofer-Institut für Kurzzeitdynamik, Ernst-Mach-Institut (EMI), Freiburg, Germany, Report E 43/99, 1999.

[29] Nahme, H. Equation of state measurements of 9SMn28- and C45-steel. Fraunhofer-Institut für Kurzzeitdynamik, Ernst-Mach-Insitut (EMI), Freiburg, Germany, Report E 11/91, 1991.
[30] Kuchling, H. Taschenbuch der Physik. Carl Hanser Verlag.
[31] Johnson, G.R., Cook, W.H.. Fracture characteristics of three metals subjected to various strains, strain rates, temperatures and pressures. Eng. Frac. Mech., 1985, 21 (1), p. 31.
[32] Yadav, S., Ramesh, K.T. The mechanical properties of tungsten-based composites at very high strain rates, Mat. Sci. Eng., 1995, A203, pp. 140-153.
[33] Dey, S., Borvik, T., Hopperstad, O.S. and Langseth, M. On the influence of constitutive relation in projectile impact of steel plates. Int. J. Impact Engng., 2007, 34 (3), pp. 464-486.
[34] Kohlrausch, F. Praktische Physik 1. B.G. Teubner, Stuttgart, 1968.
[35] Krüger, L., Meyer, L.W., Razorenov, S.W., Kanel, G.I. Investigation of dynamic flow and strength properties of Ti6-22-22S at normal and elevated temperatures. Int. J. Impact Engng., 2003, 28 (8), pp. 877-890.